



An In-Vivo Study on Nanostructured Ti Dental Implant Produced by Caliber Rolling and Surface Modification by SLActive

MOHAMMADREZA SADRKHAH,¹ GHADER FARAJI,^{1,3}
and VAHID ESMAEILI²

1.—School of Mechanical Engineering, College of Engineering, University of Tehran, Tehran 11155-4563, Iran. 2.—School of Dentistry, Aja University of Medical Sciences, Tehran, Iran. 3.—e-mail: ghfaraji@ut.ac.ir

This work researches the synchronous effect of grain refinement, induced by cold caliber rolling (CCR), and surface modification by sandblasting and acid-etching (SLA/SLActive) on the mechanical, surface, biological properties, and osseointegration improvement of commercially pure titanium (CP-Ti grade 2) dental implants. First, high-strength nanostructured CP-Ti was produced by caliber rolling. Then, SLA and SLActive surface modification methods were applied on the surface of both the CP-Ti and the nanostructured one. Surface roughness tests presented the highest value of roughness for the SLActive surface. All the specimens were implanted into the femur of six healthy New Zealand rabbits, and their properties were studied for periods of 1 and 3 months. To investigate the osseointegration, micro-CT images were tracked. Both hematoxylin and eosin (H&E) and Masson's trichrome (TRI) histopathology evaluations were conducted on all the implanted samples. Increases in bone mineral density (BMD), bone mineral content (BMC), and bone volume fraction (BV/TV) were noted. H&E histopathology indicated an increase of osteogenesis for the SLA-nano implants. TRI histopathology showed an increase in collagen secretion and bone-to-implant contact (BIC) of the SLActive implants, which demonstrated their improved osseointegration. All these results proved the effectiveness of caliber rolling and SLActive methods on the osseointegration of titanium dental implants.

INTRODUCTION

Among all bio-metals, titanium has a very high ability to bond with living bone.¹ In fact, by inserting titanium implants into the jawbone, if the implant is correctly fixed in place and no force is applied to it, after a certain period of time, a direct connection between the bone and the implant is established, without the formation of fibrous tissue. Furthermore, it should be noted that, due to the low electrical conductivity of titanium, electrochemical oxidation occurs, which leads to the formation of a passive oxide layer on its surface.² This oxide layer, in turn, creates high corrosion resistance in this metal. This oxide layer continues to exist on

titanium at high pH such as that of the human body.^{3,4} In aqueous environments, titanium and its oxides have a very low tendency to form ions and to react with macromolecules.⁴ Titanium and its alloys are used to replace a hard part of the body that has been damaged, disabled, or injured.

The unfavorable mechanical properties of commercial pure titanium (CP-Ti) have limited its use in applications that require mechanical strength. For this reason, the use of Ti-6Al-4V titanium alloy has expanded. Despite the widespread use of titanium alloy in implants, studies show that this alloy can release aluminum and vanadium ions.⁵ In fact, vanadium produces high cytotoxicity and aluminum may induce senile dementia.⁶ Allergic and cytotoxic effects and neurological disorders might be induced by these released ions. Therefore, the need to replace Ti-6Al-4V with a suitable biomaterial should be seriously studied. CP-Ti could be the best choice

(Received May 25, 2023; accepted July 24, 2023;
published online August 25, 2023)

to replace Ti-6Al-4V; however, using this material in dental implants could cause failure of the implantation process caused by its low mechanical properties.^{7,8}

Therefore, in order to use CP-Ti in implants, its mechanical properties must be improved. Various works⁹⁻¹³ have demonstrated the beneficent effect of severe plastic deformation (SPD) methods on the mechanical and biological properties of ultrafine-grained (UFG) and nano-structured CP-Ti, among them, higher mechanical strength,^{14,15} enhanced corrosion resistance, developed growth of bone tissues, and acceleration of bone treatment. In fact, by taking advantage of this method, very high plastic strains are imposed on metal materials, which cause significant grain refinement in them.^{9,16-19}

Among all SPD techniques, equal channel angular pressing (ECAP) is the most well-known, and several researchers have previously shown its beneficial effects on the mechanical and biological characteristics of CP-Ti.^{20,21} However, with its current form, it has very little chance to be used in the industry. One of the reasons is its capability to produce materials with limited size. Also, a variety of rods and wires can be produced using a process called caliber rolling. The most important feature of this process and the whole rolling process is its high production speed. Krallics et al.¹⁶ applied warm caliber rolling on CP-Ti grade2 at a temperature of 450°C and, moreover, they took advantage of round-shaped rollers. At the end of the process, a UFG microstructure was achieved, possessing enhanced mechanical properties. In fact, by doing this study, they presented the great feasibility of this method to improve the mechanical properties of CP-Ti. Also, in another work, Ti-13Nb-13Zr alloy was processed by multi-pass caliber rolling, at a temperature of 650°C, by Lee et al.¹⁷ A near-UFG microstructure and improved mechanical properties were reported by them. Furthermore, Lee et al.²⁰ carried out multi-pass caliber rolling on Ti-6Al-4V titanium alloy, producing a UFG microstructure. After rolling, a microstructure containing grains with a size of 0.2 μm was obtained. In addition, this UFG alloy exhibited improved mechanical properties and good formability. Doiphode et al.²¹ processed the Mg-3Al-1Zn (AZ31) alloy by caliber rolling. Again, grain refinement occurred and a significant increase in tensile behavior, with a small decrease in deformability, were observed.

Besides the effect of grain refinement on the mechanical properties of metal materials, especially CP-Ti, several studies have been carried out to investigate the effectiveness of grain refinement on the biological response of cells.²² Kim et al.²³ studied the biocompatibility of ultra-fine-grained CP-Ti in vitro. Samples of titanium grade2 were ECAP-ed and, in addition to the strength, the cell-substrate interactions were improved. In fact, biocompatibility, wettability, and cell proliferation were higher

compared to coarse-grained Ti (CG-Ti). In another work, CP-Ti grade4 was grain-refined by Valiev et al.²⁴ They investigated the effect of grain refinement on the cytocompatibility with fibroblast cells. The result of this work exhibited a faster osseointegration process for UFG-Ti compared with CP-Ti.

Additionally, there have been several surface modification methods carried out on the surface of implants in order to present an improved wettability, enhanced cell-implant adhesion and cell proliferation, and faster osseointegration process.²⁵ All these properties result in a shorter treatment duration. Therefore, the surface roughness of titanium implants was considered as a factor that can affect the rate and quality of osseointegration and biomedical fixation.^{26,27} Physical modification of the surface of titanium dental implants can alter the surface morphology and increase the surface roughness in the microscale, which is advantageous for the rapidity of the osseointegration process.²⁸ The most common physical technique to modify the surface is sandblasting.²⁶ Aluminum oxide, titanium oxide, and hydroxyapatite are normally used for sandblasting titanium dental implants. Various studies have shown that sandblasting using titanium oxide particles causes an increase in the bone-to-implant contact (BIC) value in titanium implants.^{29,30} Also, in other works, it has been shown that sandblasting using aluminum oxide and titanium oxide causes the same result in the value of BIC, which confirmed that the biomechanical stability of sandblasted implants was higher than implants with polished surfaces.³¹ Also, in another research, biomineralization of bone-like hydroxyapatite in order to improve the mechanical and osteoblastic performance of poly scaffolds was investigated, and it resulted in an increase in cell viability and rapid apatite formation in mineral solution.³² The same researcher worked on multiple mechanisms for efficient and long-term filtration of fine particulate matters.³⁰ Also, chemical surface modification methods like acid-etching create micropits on the surface of the implants which are useful to increase surface energy, cell adhesion, protein adsorption, and eventually boost the speed of the osseointegration process.^{33,34} Today, the surface of many titanium implants is modified by combining both sandblasting and acid-etching techniques (SLA/SLActive).^{31,35} These surface modification methods combine the advantages of sandblasting and acid-etching to provide a micro-rough surface. In order to modify the surface by the SLA (sandblasted/large-grit/acid-etched) technique, first the surface of implant is struck by stiff particles, after which the surface is acid-etched. This can establish a modified surface which is feasibly identifiable by living cells and therefore prompting a rapid osseointegration.³³ Owing to a high rate of osteoblast proliferation and cell adhesion at the surface of titanium dental implants, an SLA-modified surface results in enhanced BIC.³⁴ Furthermore, another

technique known as SLActive induces a more accelerated bone formation and a higher BIC compared to the SLA method.³⁶ The SLA and SLActive modification methods are applied in a similar way on the surface of titanium dental implants, excepting the last step. After acid-etching, the SLA implant is dried and packed to use, but the SLActive one is cleaned under the protection of N₂ gas and packed in a saline solution (NaCl). Rubb et al.³⁷ demonstrated more hydrophilicity and a higher surface energy of SLActive implants compared to SLA ones as a result of the last step of the SLActive process. Shalabi et al.³⁸ described that a stronger living cell response and bone tissue reaction in the first stages of bone healing were facilitated by a higher surface energy and hydrophilicity. Masrouri et al.³⁹ investigated the biocompatibility in vivo of SLA and SLActive of CP and UFG-Ti grade2 processed by equal channel angular pressing, and, by applying different tests, they found that the most rapid bone healing belonged to UFG-Ti grade2 surface modified by the SLActive technique. Sadrkhah et al.⁴⁰ studied the effect of the SLA and SLActive methods on the wettability and cell adhesion of CP and UFG-Ti grade2 processed by equal channel angular pressing. They confirmed that the best wettability and cell adhesion occurred for the UFG-Ti grade2 surface modified by SLActive. Schwartz et al.⁴¹ researched the osseointegration difference between SLA and SLActive implants by histological tests. A greater BIC and higher bone density were achieved for the SLActive implant, 2 weeks following the implantation. Most of the works presented above used equal channel angular pressing, which is a laboratory-scale process for grain refinement.

Caliber rolling is a continuous deformation method suitable for industrial production of UFG and nanostructured materials. The main purpose of this study is to investigate the effectiveness of the grain refinement by the cold caliber rolling (CCR) method which is a continuous deformation method suitable for mass production of UFG Ti for improving the mechanical properties of CP-Ti grade2. At the same time, the effect of the SLActive surface modification method in increasing the bioactivity and speed of the osteointegration process was examined using different tests. Therefore, in this study, an attempt was made to provide the appropriate material in terms of mechanical strength for manufacturing implants using the CCR method. Also, for the first time, the SLActive surface modification method has been applied to rolled titanium to investigate its ability to improve its biological properties. In order to achieve this purpose, for in vivo testing, implants made of CG-Ti and UFG-Ti grade2 were placed in the femurs of a number of rabbits. Then, to study the interaction between the implant and the bone, biological tests were performed on the samples.

MATERIALS AND METHODS

Specimen Preparation

In order to start the work, rods of CP-Ti grade2 (Fig. 1a) with a length of 350 mm and diameter of 12 mm, as depicted in Fig. 1b, were prepared using a wire-cutting machine. Next, by using a caliber rolling machine (Fig. 1c), offered by the center for processing and characterization of nanostructured metals at the University of Tehran (Tehran, Iran), the starting material (CP-Ti) was processed. In fact, this machine consisted of eight deformation passes in which oval and circular grooves are created one by one. The starting rod entered the first pass, which was oval, and it was immediately rotated 90° when it was introduced to the second groove, which was circular. This process continued to the last groove which was circular, all of this work being fulfilled at room temperature. Finally, the caliber rolling machine turned the initial piece into a rolled sample with a diameter of 5 mm and a length of 2000 mm, as shown in Fig. 1d. All the characteristics of the CCR machine grooves are shown in Fig. 1c and the total reduction of area was determined as ~83%. To prepare the material for in vivo testing, implant screws were designed and manufactured based on the standard ASTM F543, so that the outer diameter and screw length were 3 mm and 6.5 mm, respectively (Fig. 1e). These implants were made out of CP-Ti and the rolled one which, in this work, have been designated as CG-Ti and nano-Ti, respectively.

SLA and SLActive Procedure

After preparing the implant specimens, in order to modify their surface, the samples were subjected to SLA and SLActive techniques (Fig. 2). To perform both of these methods, first the samples were sandblasted using hard alumina particles whose particle size was ~200–180 μm. The appropriate distance between the sample and the sandblasting nozzle was about 100 mm, and all the samples were sandblasted under an air pressure of 0.5 MPa for approximately 5 min. Due to the possibility of the presence of alumina particles on the surface of the implant, the sample was cleaned for 5 min in an ultrasonic cleaner machine containing some deionized water and alcohol. Then, the samples were chemically etched in a solution of 3 acids (37wt% HCL:98wt% H₂SO₄:H₂O, 2:1:1) for 5 min. Up to this point (stage 3 in Fig. 2), all the stages were performed similarly for both techniques. Afterward, different steps were taken for the SLA and SLActive techniques. For the SLA method, the samples were washed in an ultrasonic device containing a fresh solution of distilled water and alcohol. This step was carried out at room atmosphere and the implant samples were stored dry in a container (stage 4 in Fig. 2). However, for the SLActive method, the samples were cleaned by an ultrasonic device

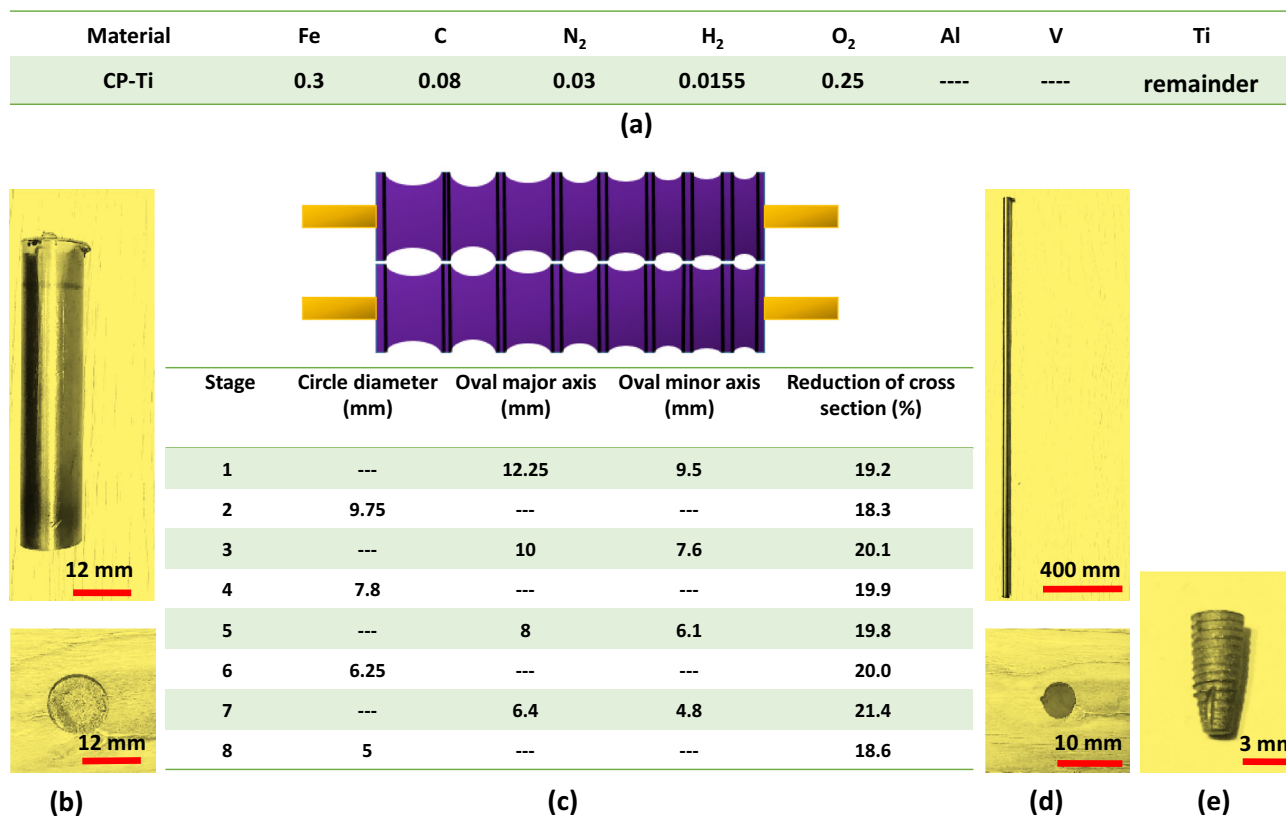


Fig. 1. (a) Chemical composition of material (%wt), (b) schematic of CG-Ti (as-received), (c) caliber rolling and characteristics of each groove, (d) nano-Ti (as-rolled), and (e) dental implant turned by computer numerical control machining.

containing distilled water and alcohol solution, in a vacuum chamber under nitrogen gas (stage 4 in Fig. 2). Then, the samples were stored inside a capsule containing NaCl (saline), under the same vacuum conditions (stage 5 in Fig. 2).

Thus, specimens studied in this work were classified as: CP-Ti (CG-Ti), SLA CP-Ti (SLA-CG-Ti), SLActive CP-Ti (SLActive-CG-Ti), rolled CP-Ti (nano-Ti), SLA rolled CP-Ti (SLA-nano-Ti), and SLActive rolled CP-Ti (SLActive-nano-Ti).

Microstructural Evolutions and Mechanical Properties of Nano-Ti

In order to investigate the microstructural changes caused by applying the rolling caliber on CG-Ti, and also grain sizes, the microstructures of CG-Ti and nano-Ti was studied by scanning electron microscopy (SEM; S-4160; Hitachi; 20 kV). For this purpose, small samples were cut from the CG-Ti and nano-Ti in the rolling direction. Then, their surfaces were finished using SiC papers (500–3000), under tap water. Next, to prepare specimens for SEM, they were acid-etched by a solution of acid (HNO₃:HF:H₂O, 10:2:88). Grain sizes were estimated by using image analysis software, ImageJ. To clarify the mechanical properties of the nano-Ti, an Instron universal tensile machine was used. To this end, tensile test samples, according to ASTM

E8 requirements, were cut out of the CG-Ti and nano-Ti in the rolling direction. This test was accomplished at a strain rate of 0.001 s⁻¹.

Characterization of SLActive-Modified Surface

The surface morphology of the nano-Ti implant, as-machined, as-sandblasted, and as-sandblasted + acid-etched (SLA and SLActive), was investigated by a field-emission scanning electron microscope (FESEM; DSM 960A; Zeiss, Germany). Using a surface roughness testing machine (Hommler Werke, T8000, Germany), the surface roughness was clarified for CG-Ti, SLA-CG-Ti, SLActive-CG-Ti, nano-Ti, SLA-nano-Ti, and SLActive-nano-Ti specimens.

In-vivo Biocompatibility Test

Preparation of Animals

In order to conduct in vivo tests, the implants should be introduced into the living body. Thus, six healthy and mature New Zealand rabbits were selected (Production and Research Complex Pasteur Institute of Iran, Karaj, Iran) weighing almost 3–3.5 kg and at 9–12 months old. The rabbits were placed in separate cages and provided with sufficient food and water. To adapt the rabbits to the new

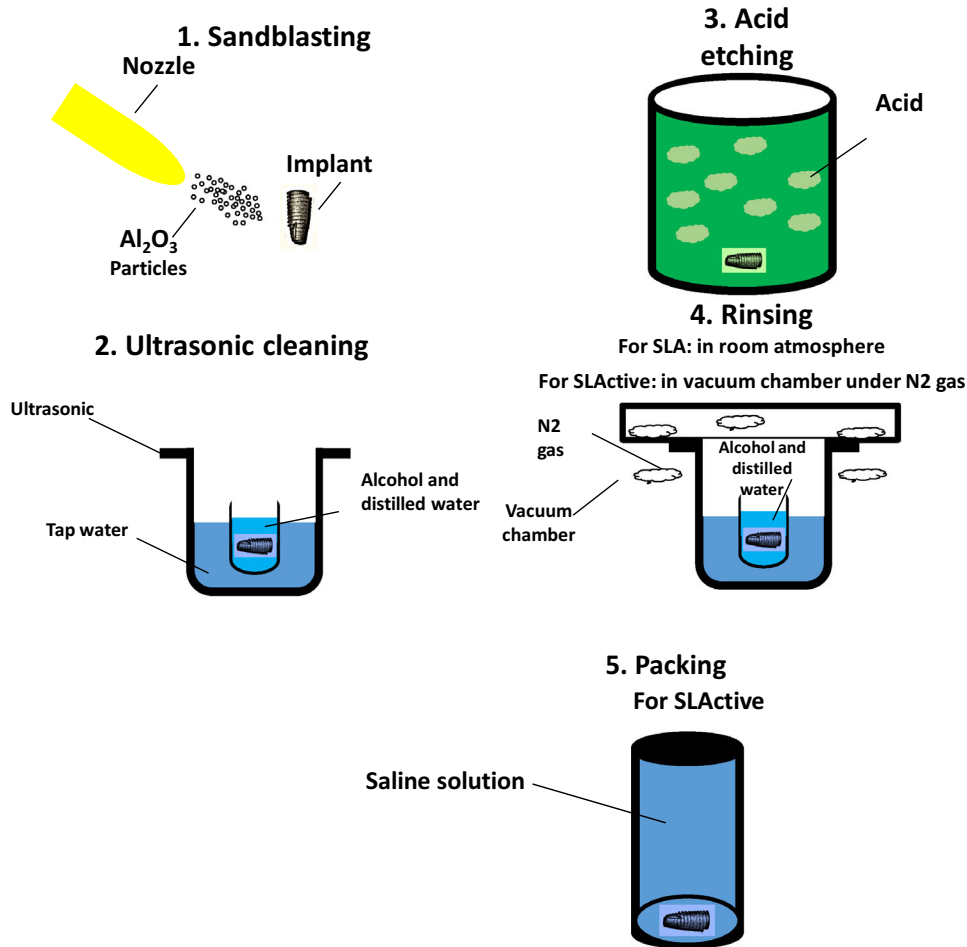


Fig. 2. SLA and SLActive surface modification methods on the dental implant.

environment, they were kept in a special pen, and the implants were inserted into the (c) bone of the left femur and (b) bone of the right femur of the rabbits 10 days before surgery. They were not fed 12 h before surgery. First, the animals were generally anesthetized by a femoral muscle injection of ketamine 10% (5 mg/kg) and xylazine hydrochloride 2% (2 $\mu\text{g}/\text{kg}$). Next, isoflurane anesthetic gas was applied to complete the anesthesia state. To prepare the rabbits for the surgery, their leg hair was shaved and surgical scrub (7.5% butadiene soap and then 10% butadiene) was applied to them. All this process was performed under sterile conditions.

Implantation of Samples into the Rabbits' Body

To discuss the osseointegration property of all the implants with different surface characteristics, they were inserted in the femur of these six rabbits. To achieve this goal, all the implants must have been sterilized. Accordingly, they were totally subjected to formalin tablets for 24 h and then placed in capsules containing saline. Also, to preserve the implants in the presence air, a protective gas, N_2 ,

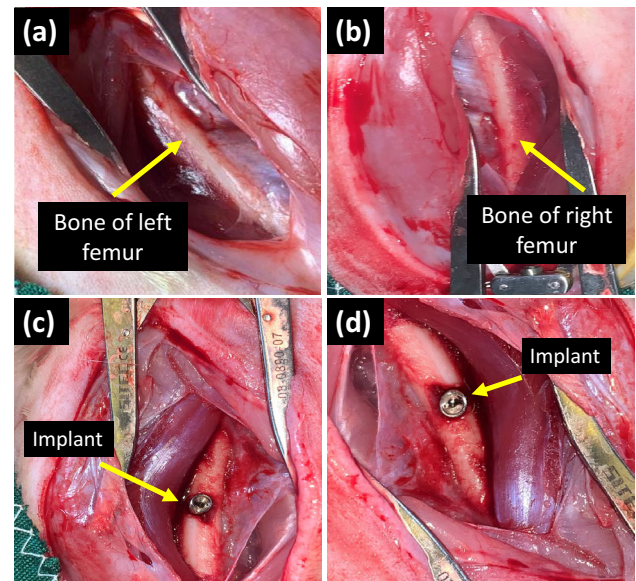


Fig. 3. Incision of rabbit femurs: (a) bone of left femur, (b) bone of right femur, (c) and (d) after implantation.

was used. When the animals were anesthetized, the preparation of the hind limbs started by longitudinal incisions of 4–5 cm using a surgical scalpel. To access the femur bone, the muscular part of the limbs was dissected (Fig. 3a and b). Once the bone of the femurs became visible, using a drill with a diameter of 2 mm (coordinated with the size of the implants), one hole in the left femur and one in the right femur were gradually drilled. It should be noted that the implantation areas were continuously rinsed by normal saline solution. All the implants were inserted (Fig. 3c and d) consecutively in the right and left femurs, and this and the order of implantation are given in Table I. The implantation was accomplished at a torque of 10 N cm. Once the implantation process was completed, the torn muscles were stitched with Vicryl 0-4 biodegradable surgical sutures, stitching the sub-skin layer (skin) with biodegradable surgical suture 0-4, and, finally, to stitch the skin of the animal, the nylon surgical suture was consumed. After the surgery had finished, all animals were cautiously kept under observation and fed sufficiently. Enrofloxacin injections were used to avoid eventual infection. For this purpose, a solution of 0.5 ml enrofloxacin and 1.5 ml deionized water were injected into the animals once a day for 3 days. Also, each day for 2 days following the implantation, the rabbits were injected with 1 mg tramadol in order to suppress their pain. It should be noted that the incised areas were constantly under surveillance and, when the implantation area healed, the skin stitches were eliminated 15 days after the surgery. By stopping the hearts of animals by a high dose of pentobarbital, they were euthanized after 4 and 8 weeks following the surgery, according to the living animal test protocol. To perform micro-computed tomography (Micro-CT) and histopathology tests, the implanted femurs were detached. When the femurs were separated, to retain them for subsequent tests, they were put in formalin solution (H₂O, 1:10). From this part onwards, the implants retained in the living animal's femur for 1 month and 3 months have the digits 1 or 3, respectively.

Micro-Computed Tomography (Micro-CT)

To investigate new bone formation around the implanted specimens, micro-CT tests were performed for all the inserted implants. To this end, an in vivo micro-CT scanner (LOTUS in-Vivo; Behin Negareh, Tehran, Iran) was used. The scanner had a cone beam micro-focus x-ray source and a flat panel detector. In order to obtain the best possible image quality, the x-ray tube voltage and its current were set to 80 kV and 40 μA, respectively and the frame exposure time set to 2 s with × 4 magnification. Total scan duration was 49 min. Slice thicknesses of reconstructed images were set to 20 μm. All the protocol settings process was controlled by LOTUS-in-Vivo-ACQ software. The acquired 3D data were reconstructed using LOTUS in-Vivo-REC by a standard Feldkamp–Davis–Kress algorithm. Also, LOTUS in-Vivo-3D was used for rendering of the reconstructed images and, by adding the Bone Analysis Plugin inside the software, the BMC (g) (bone mineral content), BMD (g/cm²) (bone mineral density), and BV/TV (%) (bone volume fraction:bone volume/total volume) parameters have been reported.

Histopathology Study (Hematoxylin and Eosin (H&E) Stain)

First, following the micro-CT investigations, the implants were removed from the surrounding bone, then the left and right femurs of all the rabbits were cut into 2-mm-thick sections. Incisions were made in the transverse section of each femur. Sections were prepared from the bone surrounding the near-apex area of the implants. Then, they were all fixed with 10% buffered formalin. Next, the bone sections were dehydrated in ascending concentrations of alcohol (100% alcohol to deionized water) and embedded in paraffin wax. Sections of 4 μm were sliced and placed on glass slides. In order to continue the preparation of the histopathology samples, deparaffinization was completed and rehydration was applied by rinsing with xylene for 15 min and tap water for 5 min. Finally, in order to study the new bone formation and the osteogenesis

Table I. Order of implants inserted in the femurs of rabbits and their designation

<u>Rabbit number</u>	<u>Implant designation</u>	<u>Femur</u>	<u>Duration (month)</u>
1	1-CG-Ti	Right	1
	1-SLA-CG-Ti	Left	1
2	1-SLActive-CG-Ti	Right	1
	1-nano-Ti	Left	1
3	1-SLA-nano-Ti	Right	1
	1-SLActive-nano-Ti	Left	1
4	3-CG-Ti	Right	3
	3-SLA-CG-Ti	Left	3
5	3-SLActive-CG-Ti	Right	3
	3-nano-Ti	Left	3
6	3-SLA-nano-Ti	Right	3
	3-SLActive-nano-Ti	Left	3

percentage, the slides were put into H&E staining solution, and, to clarify the collagen fibers and BIC values, slides were rinsed in Masson's trichrome staining solution. Imaging was performed by an optical microscope (LABOMED), and number of the osteocytes and BIC values were calculated by image analysis software, ImageJ.

Ethics

This study was performed in total accordance with the instructions of the animal's clinic, under the supervision of the Faculty of Pharmacy, Tehran University of Medical Sciences. All implantation surgeries were carried out under Isoflurane Anesthetic Gas and the best was done for the reduction of animals' pain endured by implantations.

RESULTS AND DISCUSSION

Microstructural and Mechanical Characteristics of Nano-Ti

By applying all 8 passes of CCR on CG-Ti, nano-Ti was attained. The microstructure of these samples was investigated by SEM. As depicted in Fig. 4a, the microstructure of Ti-gr2 had coarse grains that were scattered throughout the structure with a size of ~ 20 μm . Nevertheless, the image obtained for the nano-Ti (Fig. 4b) sample show that, due to cold rolling and considerable imposed plastic deformation, grain refinement occurred and their size decreased to ~ 90 nm. In fact, these images describe the efficiency of the CCR in grain refinement of CG-Ti and, therefore, a nano-structured material. The tensile test results for CG-Ti and nano-Ti are depicted in Fig. 4c. In fact, by imposing 8 passes of the CCR process, the grain size of CG-Ti decreased, its microstructure was refined, and, according to the well-known Hall–Petch relationship, the mechanical strength was improved. As is illustrated in Fig. 4c, the yield and tensile strengths of CG-Ti were approximately 400 and 460 MPa, respectively, while, by CCR, these values augmented to nearly 780 and 875 MPa for nano-Ti, which presented 95% and 90% increase in yield stress (YS) and ultimate tensile strength (UTS) compared to CG-Ti. Nevertheless, the formability of nano-Ti decreased to 0.15 from an initial value of 0.25 for CG-Ti. Practically, for almost all grain-refining methods, solute atoms are important factors in strengthening of metals, in which they agglomerate at grain boundaries (GBs) and function as barriers and confront dislocation motion.⁴² On the other hand, by imposing the CCR method, the volume of vacancies and defects and new GBs could be increased, resulting in metal strengthening.⁴³

Surface Characteristics

Morphology of Modified Surfaces

FESEM images of the nano-Ti implant, as-machined, as-sandblasted, and as-SLA and as-SLActive,

surfaces are depicted in Fig. 5. As can be derived from this figure, the modified surfaces had different forms compared to machined surfaces (Fig. 5a). The surface homogeneity presented on the surface of the sandblasted implant was an outcome of the sandblasting uniformity throughout the surface which, at the end, resulted in homogeneity of the SLA and SLActive modified surfaces. Therefore, in this way, the surface properties were the same at all points. It should be noticed that the SLA and SLActive surfaces are only chemically different and, therefore, their surface topography might be similar. By referring to Fig. 5c and d, this topic is clearly demonstrated. Considering the morphology of the surface, osseointegration is a crucial factor for the success of a dental implant. This parameter is in a tight relationship with the surface morphology of a dental implant. Numerous researches have been performed to describe the relationship between the surface quality and the osseointegration process.^{44,45} In fact, in all of these works, it was demonstrated that, by creating micropits and micro-pores on the surface of an implant, the contact area between the bone and the implant improved which lead to a better and faster osseointegration.⁴⁵ As can be seen in Fig. 5b, by applying sandblasting on the surface of the nano-Ti implant, the surface was divided into sections of broken surfaces. Nevertheless, by the acid-etching process, these broken edges were transformed to corroded edges (Fig. 5c and d).

Roughness of Modified Surfaces

The roughness parameters, R_a (arithmetic mean deviation of the profile), R_q (square of root average for a detected profile), and R_z (maximum height of the profile), were derived by a roughness testing machine and are shown in Table II. The surface roughness of all the samples increased compared to the machined ones.

Different works have proved the existing direct relationship between surface roughness and living cell behavior.^{44,46} Moreover, CG-Ti was more susceptible to SLA and SLActive because of its lower strength and higher ductility compared with nano-Ti. Also, it should be mentioned that the R_z for CG-Ti was clearly higher than that for nano-Ti, which means that the nano-sample had a smoother surface. Nevertheless, it should be considered that the surface quality is not the only agent affecting the surface properties of a material. Also, the values of roughness for SLActive surfaces were higher compared to their SLA counterparts, which could be effective in establishing a high BIC value and so a better osseointegration.^{47,48}

Micro-Computed Tomography (Micro-CT)

3D micro-CT images of all the implants studied in this work are shown in Fig. 6a. Information on new bone formation and the osseointegration process, and

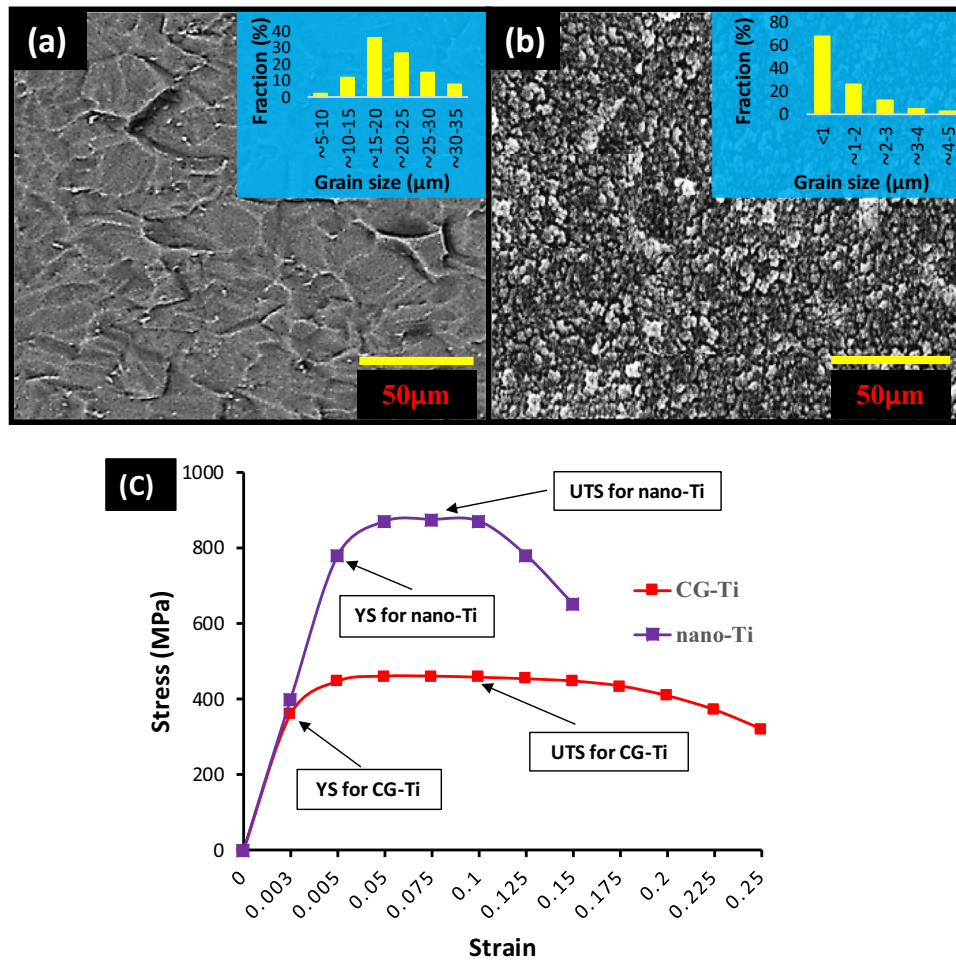


Fig. 4. SEM images and grain size distribution of (a) CG-Ti and (b) nano-Ti, and (c) tensile test results for CG-Ti and nano-Ti.

also the microstructure of the trabecular bone surrounding the implants, are presented by this figure. According to the 1-month specimens' micro-CT (Fig. 6-a(a1-b3)), the SLA and SLActive specimens offered more new formed bone compared to their unmodified counterparts. On the other hand, the osseointegration process was more improved for the nano-Ti (Fig. 6-a(b1)) sample compared to the CG-Ti (Fig. 6a(a1)) one. Furthermore, the 3-month specimens were more osseointegrated compared to their 1-month counterparts. These results were derived schematically from Fig. 6. However, in order to obtain more exact results, the values of the bone regeneration parameters, i.e., BMD, BMC, and BV/TV, were calculated and are shown in Fig. 6b and c. In order to find these values, micro-CT imaging was performed for all the samples. The BMD values for all the implants are shown in Fig. 6b. This important parameter describes the amount of bone mineral in the bone tissue and is an indicator of osteoporosis and fracture risk.⁴⁶ According to this figure, 1-SLA-CG-Ti and 1-SLActive-CG-Ti had no large difference in the amount of BMD.

However, for the 3-month specimens, i.e., 3-SLA-CG-Ti and 3-SLActive-CG-Ti, this difference was increased. Also, it should be noticed that the 3-month specimens had higher BMD compared to the 1-month ones. The 3-SLActive-nano-Ti implant had the highest BMD among all the specimens. More bone formation in this implant could be as a result of containing more pores and irregularities on the surface. In fact, this result showed that the surface area of this implant was the largest compared to the other, which resulted in more new bone formation and a higher BMD value. Figure 6b shows the BMC values for all the specimens investigated in this work. As can be derived from this figure, the BMC of the SLA and SLActive specimens were significantly higher than their unmodified counterparts. This result confirmed the efficiency of these surface modification methods on new bone formation and the osseointegration process of these implants. Additionally, the 3-SLActive-nano-Ti presented the highest amount of BMC, as was the same for the BMD value. Therefore, these values of BMD and BMC for the 3-SLActive-nano-Ti

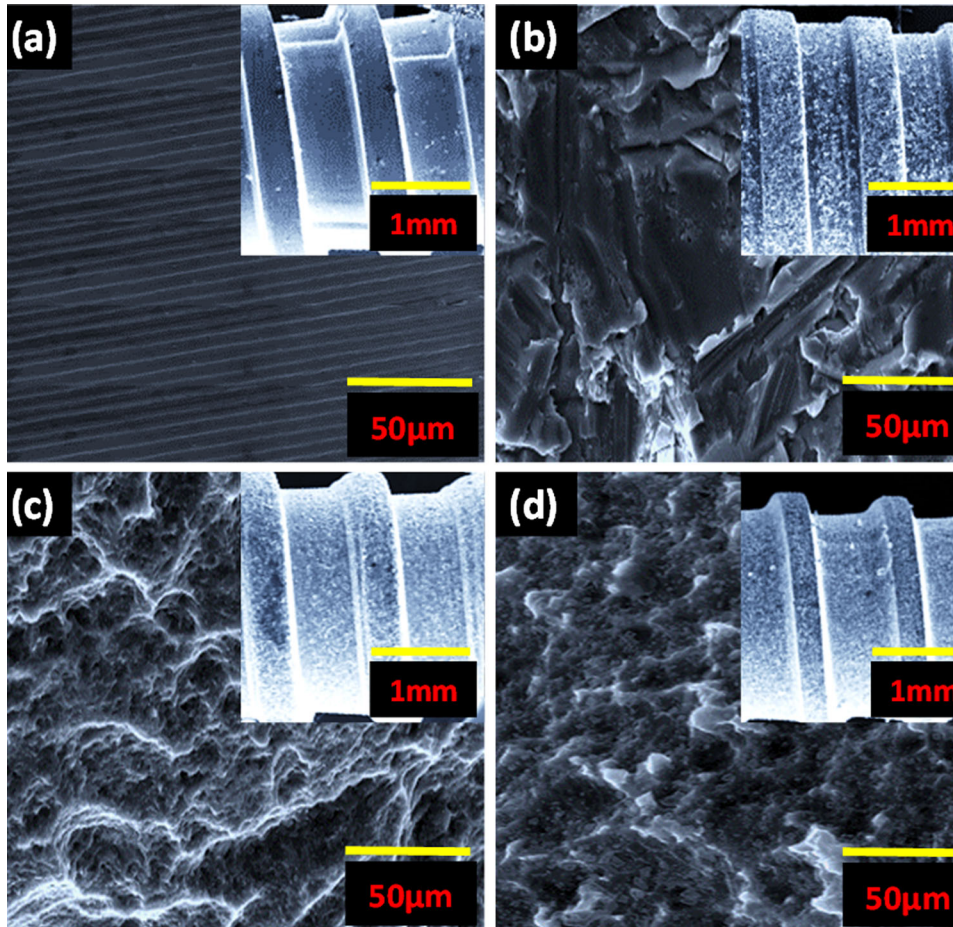


Fig. 5. FESEM images of the nano-Ti implant surface as: (a) machined, (b) sandblasted, (c) sandblasted + acid-etched (SLA), and (d) sandblasted + acid-etched (SLActive). Alterations in the topography of the surface-modified implants occurred.

Table II. Surface roughness parameters of all implants ($n = 5$)

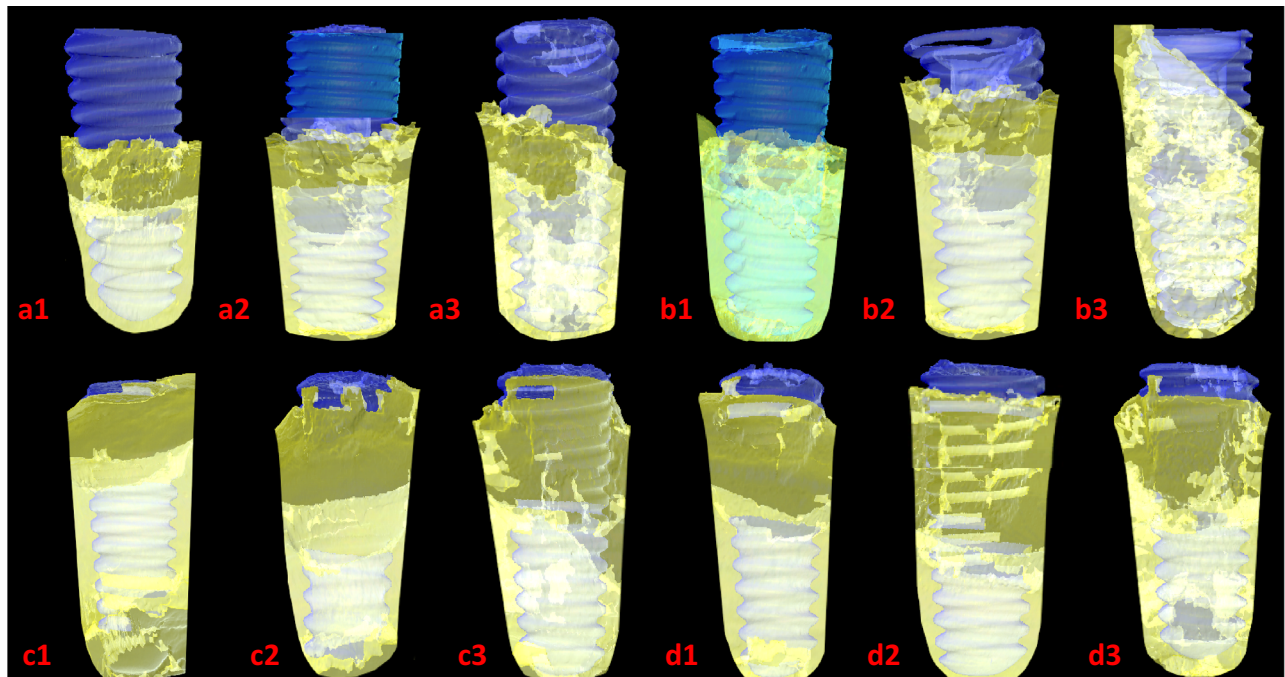
Process	R_a (μm)	R_q (μm)	R_z (μm)
Polished (all samples)	0.05 ± 0.07	0.09 ± 0.4	3.75 ± 0.92
SLA-CG-Ti	1.95 ± 0.03	2.43 ± 0.26	28.16 ± 0.17
SLActive-CG-Ti	2.92 ± 0.08	3.95 ± 0.02	38.44 ± 0.62
SLA-nano-Ti	1.84 ± 0.04	3.37 ± 0.19	24.62 ± 0.99
SLActive-nano-Ti	2.97 ± 0.05	4.17 ± 0.12	37.32 ± 0.25

could advantageously induce bone formation in the area surrounding the implant. Moreover, the BV/TV amounts illustrated in Fig. 6c showed a significant increase for the implants after 3 months of implantation compared to the implants after 1 month of implantation. Also, it should be mentioned that the BV/TV for the 1-nano-Ti and 3-nano-Ti samples was higher than that of the 1-CG-Ti and 3-CG-Ti, importantly confirming the positive effect of grain refinement in improving the biological contact between the implant and the living bone. However, by applying the SLA surface modification method, no considerable

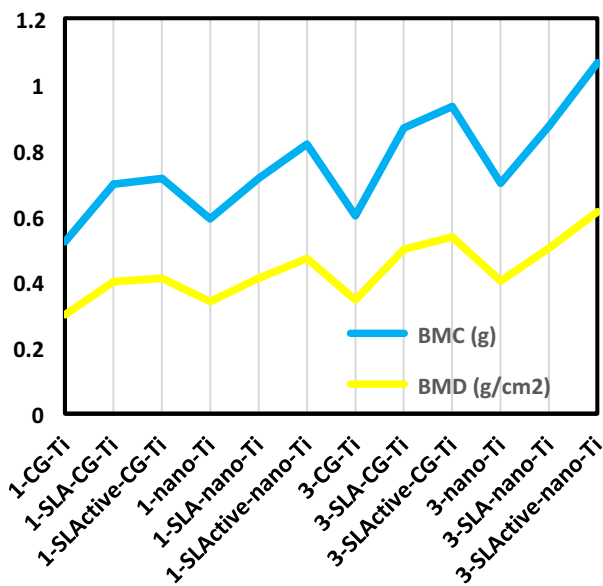
difference was observed between the 1-SLA-CG-Ti and 1-SLA-nano-Ti implants. In spite of that, the BV/TV for 3-nano-Ti was obviously higher than that of 3-Ti-gr2 specimens. It was found that the maximum value of the BV/TV, the volume of mineralized bone per unit volume of implant, was directly related to the surface characteristics of the implants.

Histopathology Report (H&E)

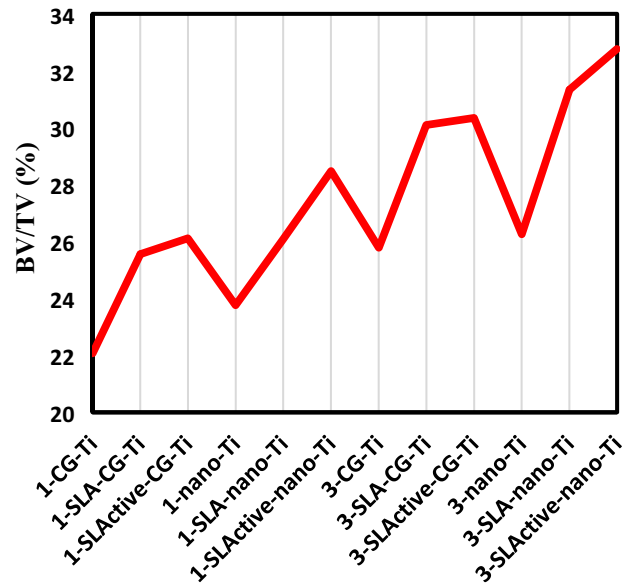
The images in Fig. 7 show a longitudinal section of bone tissue stained with H&E. In this staining, the connection of the cells with the extracellular matrix can



(a)



(b)



(c)

Fig. 6. (a) Micro-CT images of the new bone formation in the peri-implant area for 1-CG-Ti (a1), 1-SLA-CG-Ti (a2), 1-SLActive-CG-Ti (a3), 1-nano-Ti (b1), 1-SLA-nano-Ti (b2), 1-SLActive-nano-Ti (b3), 3-CG-Ti (c1), 3-SLA-CG-Ti (c2), 3-SLActive-CG-Ti (c3), 3-nano-Ti (d1), 3-SLA-nano-Ti (d2), 3-SLActive-nano-Ti (d3), (b) BMC and BMD, and (c) BV/TV values for all the implants.

be seen in the form of parallel fibers. The Haversian canal (H), which is the passage of blood vessels and connective tissue, can be distinguished in all parts of the mature bone (M). As the main cells of mature bone tissue, osteocytes (OC) were locked inside their lacuna in a needle-shaped form, and can be seen in large

numbers throughout the mature bone. The lacuna of these cells was clearly defined and immature bone had fewer osteocytes per surface unit than mature bone. Following 1 month implantation, the lowest number of osteocytes belonged to implants with unmodified surfaces. Nevertheless, the number of osteocytes was

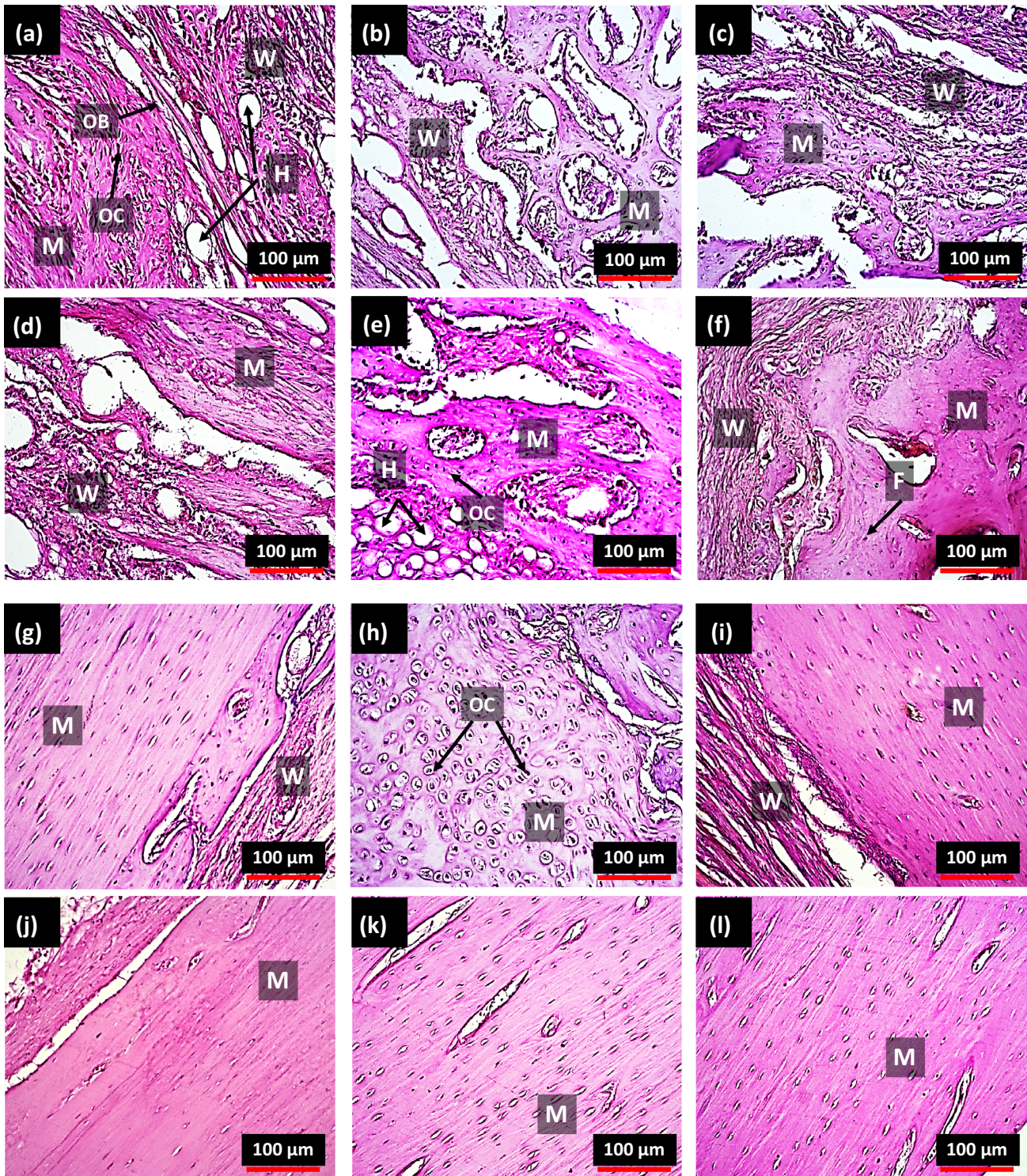


Fig. 7. H&E histopathology images for 1-CG-Ti (a), 1-SLA-CG-Ti (b), 1-SLActive-CG-Ti (c), 1-nano-Ti (d), 1-SLA-nano-Ti (e), 1-SLActive-nano-Ti (f), 3-CG-Ti (g), 3-SLA-CG-Ti (h), 3-SLActive-CG-Ti (i), 3-nano-Ti (j), 3-SLA-nano-Ti (k), and 3-SLActive-nano-Ti (l), implants. *M* mature bone, *W* woven bone, *H* Haversian canal, *C* collagen fibers inside marrow cavities, *OB* osteoblasts, *OC* osteocytes, *F* fibroblasts.

dramatically increased for the 1-SLA and 1-SLActive samples (Fig. 7b, c, e, and f) which clarified the effectiveness of these two surface modification methods. On the other hand, the presence of collagen fibers inside marrow cavities (*C*) was obvious for both the 1-SLA and

1-SLActive specimens. Furthermore, the density of mature bone was more for the 1-SLActive-nano-Ti compared to the 1-SLActive-CG-Ti sample and also the latter contained woven bone and irregularities (*W*). This result demonstrated the usefulness of both grain

refinement and the SLActive method on the osteogenesis of titanium dental implants. Moreover, the density of the mature bone was higher for the 3-month specimens compared with the 1-month ones. However, as shown in Fig. 7l, woven bone was distinguishable for 3-SLActive-CG-Ti sample which was not the case for the 3-SLActive-nano-Ti implant, which contained mature bone with osteocytes. As it can be seen for the 1-month specimens, osteoclasts are mostly present in the 1-SLActive-nano-Ti sample (Fig. 7f). For the other 1-month specimens, the osteocytes are dispersed within the woven bone. Moreover, for the 3-month samples, osteocytes have the largest presence in 3-SLA-CG-Ti, while osteoclast cells dominate the texture surrounding the 3-nano-Ti, 3-SLA-nano-Ti and 3-SLActive-nano-Ti samples. This means that the remodeling process was a step forward for the nanosamples compared to the CG ones. The osteogenesis results plotted in Fig. 8 show the percentage of osteogenesis around all the implants. As can be seen, the highest amount of osteogenesis belonged to the 3-SLActive-nano-Ti. Also, among the 1-month specimens, the 1-SLActive-nano-Ti implant presented the best osteogenesis. All these results were in direct compatibility with the surface roughness tests (Table II).

Histopathology Report (TRI)

The collagen fibers that turned blue in the TRI staining actually provide a suitable substrate for ossification and the connection of bone and implant. Therefore, the presence of collagen fibers in the first month of implantation describes the speed of the repair process of the implanted tissue (Fig. 9a, b, c, d, e, and f). The ossification of the collagen fibers further leads to an increase in the bone healing process and also helps the better adhesion of mature bone tissue to the implant.⁴⁷ Therefore, the presence of these fibers in the first month could lead to a better foundation for the function of the osteoblasts,

and, in the third month, it provided the basis for the restoration of the deposition of organic and mineral materials by the osteoblasts. Based on the results of the images obtained in the first month after placing the implant in the bone's damaged area (Fig. 9a, b, c, d, e, and f), it was found that the unmodified and SLA implants had the lowest percentage of collagen fibers compared to the SLActive ones at this time. Also, the 1-SLActive-CG-Ti implant (Fig. 9c) had a higher percentage of collagen secretion than the 1-CG-Ti (Fig. 9a) and 1-SLA-CG-Ti (Fig. 9b) samples.

On the other hand, the lowest amount of collagen was for the 1-nano-Ti sample compared to the 1-SLA-nano-Ti and 1-SLActive-nano-Ti implants, although it can be concluded that more collagen was observed around the rolled implants than round the as-received ones. In addition, based on the results obtained for the 3-month specimens, it was found that the collagen fibers were almost doubled for the nano-Ti implants compared to the as-received ones. This showed that the healing process was more rapid in the nano-Ti implants than in the as-received samples. In general, among the 3-month implants, the 3-SLActive-nano-Ti specimen had the highest percentage of collagen, and this increase was also observed for the 1-SLActive-nano-Ti. Moreover, the BIC trends which illustrate the effect of the CCR and surface modification methods on the amount of connection between the implant surface and the surrounding bone, are depicted in Fig. 10. BIC is a factor which is widely used to describe the degree of osseointegration.⁴⁸ As is shown, the highest amount of BIC for both the 1-month and 3-month implants belonged to the SLActive-nano-Ti specimens. This proved that the grain refinement induced by CCR and the increase in surface roughness can improve the osseointegration of CG-Ti implants. The BIC results confirm the osteogenesis amount illustrated in Fig. 8.

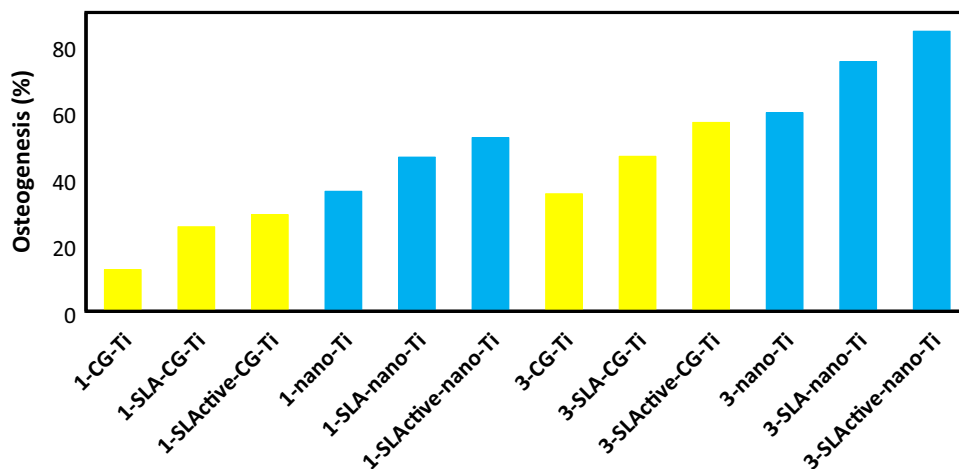


Fig. 8. Osteogenesis results calculated by image analysis for all the implants, derived from the histopathology of H&E images.

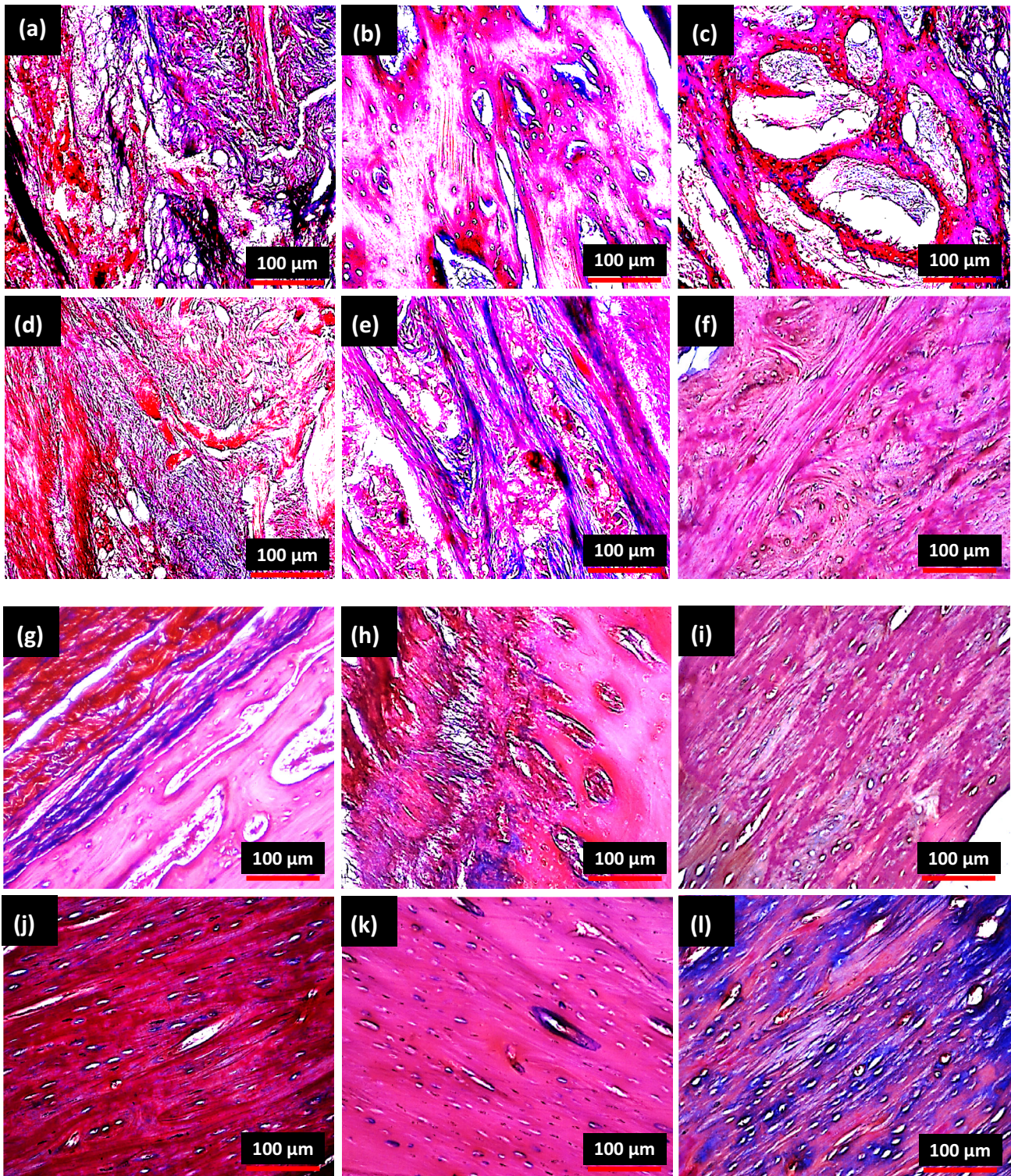


Fig. 9. TRI histopathology images for 1-CG-Ti (a), 1-SLA-CG-Ti (b), 1-SLActive-CG-Ti (c), 1-nano-Ti (d), 1-SLA-nano-Ti (e), 1-SLActive-nano-Ti (f), 3-CG-Ti (g), 3-SLA-CG-Ti (h), 3-SLActive-CG-Ti (i), 3-nano-Ti (j), 3-SLA-nano-Ti (k), and 3-SLActive-nano-Ti (l), implants.

CONCLUSION

This work intended to investigate the effect of CCR, as a conventional metal-forming method, and the SLA and SLActive surface modification

methods on the mechanical, surface and biological properties of CG-Ti. Initially, after applying CCR, grain refinement occurred and improvement in mechanical strength was achieved. Afterward, dental implants were machined from CG-Ti and nano-

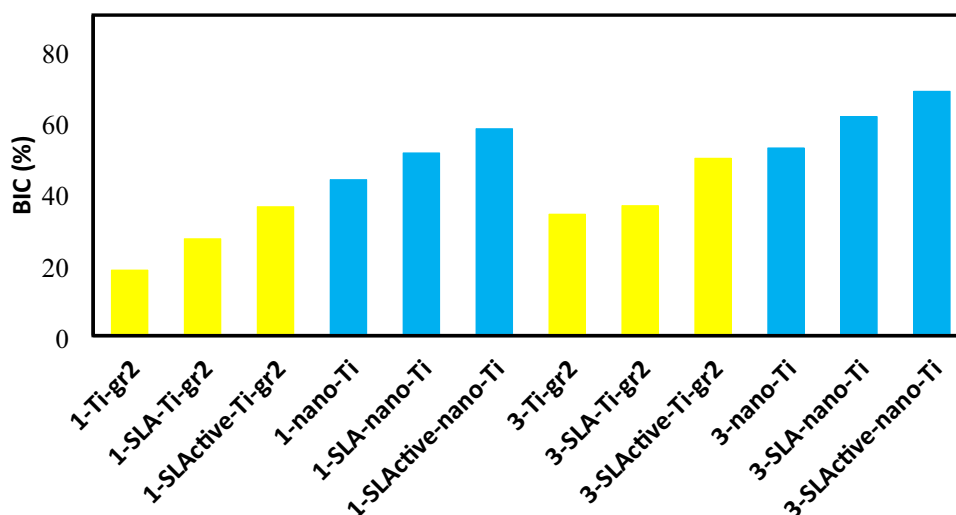


Fig. 10. Bone to implant (BIC) values for all the implants.

Ti materials and were surface-modified by SLA and SLActive. The surface morphologies of the implants were altered from the machined one, and the surface roughness test exhibited the SLActive surface as the roughest one. All 12 implants were inserted into the femur of 6 healthy rabbits to study the in vivo biocompatibility and osseointegration of each one. Micro-CT results presented the highest amounts of BMC, BMD, and BV/TV for the SLActive-nano-Ti implant for both the 1-month and 3-months. Also, more osteocytes were obvious for the 1-SLActive-nano-Ti and 3-SLActive-nano-Ti implants compared to the CG-Ti and unmodified surfaces, studied by H&E histopathology. Moreover, the best amount of osteogenesis belonged to the SLActive-nano-Ti for both the 1-month and 3-month implants. Meanwhile, the collagen secretion was assessed for all the specimens by TRI histopathology and it was clarified that collagen fibers were secreted more on the surface of the SLActive-nano-Ti samples (1 and 3 months). Additionally, the highest values of BIC for 1-month and 3-month implants belonged to the SLActive-nano-Ti specimens. All these results together indicate the effect of grain refinement induced by CCR, and the surface modification methods, SLA and SLActive, on the biological and osseointegration properties of the dental implants.

CONFLICT OF INTEREST

The authors declare that they have no conflict of interest.

REFERENCES

- M. Sarraf, E.R. Ghomi, S. Alipour, S. Ramakrishna, and N.L. Sukiman, *Bio-Design Manuf.* <https://doi.org/10.1007/s42242-021-00170-3> (2021).
- R.K. Quinn and N.R. Armstrong, *J. Electrochem. Soc.* 125(11), 1790 <https://doi.org/10.1149/1.2131295> (1978).
- N. Schiff, B. Grosgeat, M. Lissac, and F. Dalard, *Biomaterials* 23(9), 1995–2002 [https://doi.org/10.1016/S0142-9612\(01\)00328-3](https://doi.org/10.1016/S0142-9612(01)00328-3) (2002).
- P. Tengvall and I. Lundström, *Clin. Mater.* 9(2), 115–134 [https://doi.org/10.1016/0267-6605\(92\)90056-Y](https://doi.org/10.1016/0267-6605(92)90056-Y) (1992).
- J.L. Woodman, J.J. Jacobs, J.O. Galante, and R.M. Urban, *J. Orthop. Res.* 1(4), 421–430 <https://doi.org/10.1002/jor.1100010411> (1983).
- J.A. Davidson, A.K. Mishra, P. Kovacs, and R.A. Poggie, *Biomed. Mater. Eng.* 4, 231–243 <https://doi.org/10.3233/BME-1994-4310> (1994).
- W.C. Gealh, V. Mazzo, F. Barbi, and E.T. Camarini, *J. Oral Implantol.* 37(4), 499–503 <https://doi.org/10.1563/AID-JOID-09-00135.1> (2011).
- T.N. Kim, A. Balakrishnan, B.C. Lee, W.S. Kim, B. Dvornikova, K. Smetana, J.K. Park, and B.B. Panigrahi, *J. Mater. Sci. Mater. Med.* 19(2), 553 <https://doi.org/10.1007/s10856-007-3204-5> (2008).
- G. Faraji and H.S. Kim, *Mater. Sci. Technol.* 33(8), 905–923 <https://doi.org/10.1080/02670836.2016.1215064> (2017).
- R.Z. Valiev, Y. Estrin, Z. Horita, T.G. Langdon, M.J. Zechetbauer, and Y.T. Zhu, *Jom* 58(4), 33–39 <https://doi.org/10.1007/s11837-006-0213-7> (2006).
- K. Hajizadeh, B. Eghbali, K. Topolski, and K.J. Kurzydowski, *Mater. Chem. Phys.* 143(3), 1032–1038 <https://doi.org/10.1016/j.matchemphys.2013.11.001> (2014).
- F. Reshadi, G. Faraji, H. Moghtaderi, and S. Faghihi, *Jom* 72(2), 721–729 <https://doi.org/10.1007/s11837-019-03866-1> (2020).
- P. Rostami, G. Faraji, A. Sadeghi, and M. Baghani, *Trans. Indian Inst. Met.* 71(5), 1083–1090 <https://doi.org/10.1007/s12666-017-1243-2> (2018).
- M. Eftekhari, et al., *Mater. Sci. Eng. A* 703, 551–558 <https://doi.org/10.1016/j.msea.2017.07.088> (2017).
- G. Faraji and H. Torabzadeh, *Mater. Trans.* 60(7), 1316–1330 <https://doi.org/10.2320/matertrans.MF201905> (2019).
- G. Krállics, J. Gubicza, Z. Bezi, and I. Barkai, *J. Mater. Process. Technol.* 214(7), 1307–1315 <https://doi.org/10.1016/j.jmatprotec.2014.02.015> (2014).
- T. Lee, K. Park, D. Lee, J. Jeong, S.H. Oh, H.S. Kim, C.H. Park, and C.S. Lee, *Mater. Sci. Eng. A* 648, 359–366 <https://doi.org/10.1016/j.msea.2015.09.062> (2015).
- G. Faraji and H.T. Kashi, *Severe plastic deformation: methods, processing and properties* (Elsevier, 2018).
- K. Edalati, A. Bachmaier, V.A. Beloshenko, Y. Beygelzimer, V.D. Blank, W.J. Botta, K. Bryla, J. Cizek, S. Divinsky, N.A. Enikeev, Y. Estrin, G. Faraji, R.B. Figueiredo, M. Fuji, T. Furuta, T. Grosdidier, J. Gubicza, A. Hohenwarther, Z. Hor-

- ita, J. Huot, Y. Ikoma, M. Janecek, M. Kawasaki, P. Kral, S. Kuramoto, T.G. Langdon, D.R. Leiva, V.I. Levitas, A. Mazilkin, M. Mito, H. Miyamoto, T. Nishizaki, R. Pippan, V.V. Popov, E.N. Popova, G. Purcek, O. Renk, A. Revesz, X. Sauvage, V. Sklenicka, W. Skrotzki, B.B. Straumal, S. Suwas, L.S. Toth, N. Tsuji, R.Z. Valiev, G. Wilde, M.J. Zehetbauer, and Z. Zhu, *Mater. Res. Lett.* 10(4), 163–256 <https://doi.org/10.1080/21663831.2022.2029779> (2022).
20. T. Lee, D.S. Shih, Y. Lee, and C.S. Lee, *Metals (Basel)* 5, 777–789 <https://doi.org/10.3390/met5020777> (2015).
 21. R.L. Doiphode, S.V.S. Narayana Murty, N. Prabhu, and B.P. Kashyap, *J. Magn. Alloys* 1(2), 169–175 <https://doi.org/10.1016/j.jma.2013.07.005> (2013).
 22. R. Mahmoodian, S.M. Annuar, G. Faraji, N.D. Bahar, B.A. Razak, and M. Sparham, *JOM* 71(1), 256–263 <https://doi.org/10.1007/s11837-017-2672-4> (2019).
 23. T.N. Kim, A. Balakrishnan, B.C. Lee, W.S. Kim, K. Smetana, J.K. Park, and B.B. Panigrahi, *Biomed. Mater.* 2(3), S117 <https://doi.org/10.1088/1748-6041/2/3/S06> (2007).
 24. V. Polyakov, I.P. Semenova, R.Z. Valiev, and I.O.P. Conf, *Ser. Mater. Sci. Eng.* 63, 12113 <https://doi.org/10.1088/1757-899X/63/1/012113> (2014).
 25. F. Reshadi, G. Faraji, M. Baniassadi, and M. Tajeddini, *Surf. Coatings Technol.* 316, 113–121 <https://doi.org/10.1016/j.surfcoat.2017.03.016> (2017).
 26. M.E. Yurttutan and A. Keskin, *BMC Oral Health* 18(1), 1–8 <https://doi.org/10.1186/s12903-018-0509-3> (2018).
 27. C. Ivanoff, G. Widmark, C. Hallgren, L. Sennerby, and A. Wennerberg, *Clin. Oral Implants Res.* 12(2), 128–134 <https://doi.org/10.1034/j.1600-0501.2001.012002128.x> (2001).
 28. L.F. Cooper, *J. Prosthet. Dent.* 84(5), 522–534 <https://doi.org/10.1067/mpr.2000.111966> (2000).
 29. S. Lu, J. Wu, Y. Gao, G. Han, W. Ding, and X. Huang, *Int. J. Biol. Macromol.* 86, 43–49 <https://doi.org/10.1016/j.ijbiomac.2016.01.019> (2016).
 30. M. Tang, L. Jiang, C. Wang, X. Li, X. He, Y. Li, C. Liu, Y. Wang, J. Gao, H. Xu, and A.C.S. Appl, *Mater. Interfaces* 15(21), 25919–25931 <https://doi.org/10.1021/acsami.3c02365> (2023).
 31. M.D. Roach, R.S. Williamson, I.P. Blakely, and L.M. Didier, *Mater. Sci. Eng. C* 58, 213–223 <https://doi.org/10.1016/j.msec.2015.08.028> (2016).
 32. M. Tang, K. Xu, H. Shang, X. Li, X. He, L. Ke, M. Xie, Z. Zhou, C. Liu, S. Du, Y. Wang, J. Gao, and H. Xu, *Int. J. Biol. Macromol.* 226, 1273–1283 <https://doi.org/10.1016/j.ijbiomac.2022.11.240> (2023).
 33. I.S.L. Yeo, *Materials* 13(1), 89 <https://doi.org/10.3390/ma13010089> (2019).
 34. J. Alayan, C. Vaquette, S. Saifzadeh, D. Hutmacher, and S. Ivanovski, *Clin. Oral Implants Res.* 28(11), 1325–1333 <https://doi.org/10.1111/clr.12988> (2017).
 35. F. Reshadi, S. Khorasani, and G. Faraji, *Proc. Inst. Mech. Eng. Part J: J. Eng. Tribol.* 234(3), 414–423 <https://doi.org/10.1177/1350650119864246> (2020).
 36. D. Bozkaya, S. Muftu, and A. Muftu, *J. Prosthet. Dent.* 92(6), 523–530 <https://doi.org/10.1016/j.prosdent.2004.07.024> (2004).
 37. F. Rupp, L. Scheideler, M. Eichler, and J. Geis-Gerstorfer, *Int. J. Oral Maxillofac. Implants*, vol. 26, no. 6 (2011).
 38. M.M. Shalabi, A. Gortemaker, M.A.V. Hof, J.A. Jansen, and N.H.J. Creugers, *J. Dent. Res.* 85(6), 496–500 <https://doi.org/10.1177/154405910608500603> (2006).
 39. M. Masrouri, G. Faraji, M.S. Pedram, and M. Sadrkhah, *Int. J. Adhes. Adhes.* 102, 102684 <https://doi.org/10.1016/j.ijadh.2020.102684> (2020).
 40. M. Sadrkhah, G. Faraji, S. Khorasani, and M. Mesbah, *J. Mater. Eng. Perform.* <https://doi.org/10.1007/s11665-023-07928-z> (2023).
 41. L. Raines, R. Olivares-Navarrete, M. Wieland, D.L. Cochran, Z. Schwartz, and B.D. Boyan, *Biomaterials* 31(18), 4909–4917 <https://doi.org/10.1016/j.biomaterials.2010.02.071> (2010).
 42. Y.G. Ko, D.H. Shin, K.-T. Park, and C.S. Lee, *Ser. Mater.* 54(10), 1785–1789 <https://doi.org/10.1016/j.scriptamat.2006.01.034> (2006).
 43. K. Topolski and H. Garbacz, *Mater. Sci. Eng. A* 739, 277–288 <https://doi.org/10.1016/j.msea.2018.10.011> (2019).
 44. C. Pandey, D. Rokaya, and B.P. Bhattarai, *Biomed Res. Int.* 2022, 6170452 <https://doi.org/10.1155/2022/6170452> (2022).
 45. Wennerberg and T. Albrektsson, *Int. J. Oral Maxillofac. Implants*, vol. 25, no. 1 (2010).
 46. J.A. Kanis, *Lancet* 359(9321), 1929–1936 [https://doi.org/10.1016/S0140-6736\(02\)08761-5](https://doi.org/10.1016/S0140-6736(02)08761-5) (2002).
 47. J.E. Davies, *J. Dent. Educ.* 67(8), 932–949 <https://doi.org/10.1002/j.0022-0337.2003.67.8.tb03681.x> (2003).
 48. N. Lioubavina-Hack, N.P. Lang, and T. Karring, *Clin. Oral Implants Res.* 17(3), 244–250 <https://doi.org/10.1111/j.1600-0501.2005.01201.x> (2006).

Publisher's Note Springer Nature remains neutral with regard to jurisdictional claims in published maps and institutional affiliations.

Springer Nature or its licensor (e.g. a society or other partner) holds exclusive rights to this article under a publishing agreement with the author(s) or other rightsholder(s); author self-archiving of the accepted manuscript version of this article is solely governed by the terms of such publishing agreement and applicable law.